Proceedings of the
Annual Stability Conference
Structural Stability Research Council
Grapevine, Texas, April 18-21, 2012

Simulation of geometric imperfections in cold-formed steel members

V.M. Zeinoddini[1], B.W. Schafer[2]

Abstract:
In this paper, a summary of the available imperfection measurements for cold-formed steel members is presented. Three methods to simulate imperfection fields are introduced: the first is the classical approach employing a superposition of eigenmode imperfections, but scaled to match peaks in the measured physical measurements. The second is a method based on the multi-dimensional spectral representation method, in which imperfections are considered as a two-dimensional random field and simulations are performed taking a spectra-based approach. The third is a novel combination of modal approaches and spectral representation that directly considers the frequency content of the imperfection field, but employs a spectral representation method driven by the cross-sectional eigenmode shapes to generate the imperfection fields. The effect of these different approaches on the simulated strength and collapse behavior of members is investigated using material and geometric nonlinear finite element collapse modeling. The third imperfection generation method, termed the 1D Modal Spectra Method, provides an intriguing new tool in the simulation of thin-walled members.

1. Introduction

Cold-formed steel structures, like any other man-made structure have imperfections. These imperfections may be the outcome of the manufacturing process, shipping and storage, or the construction process. Geometric imperfections that are the result of the manufacturing process are the focus of this study. This type of imperfection may occur due to the coiling process, which largely influence the bow of members, or during the cold-forming process which introduces different types of imperfection: camber, twist, waviness, etc. To simulate geometric imperfections, their magnitude and distribution should be considered. This study attempts to tie the simulations into the physical reality of imperfections in cold-formed steel members. For that, first the available approaches and measured imperfection data are presented. Then, new approaches for simulating imperfections are introduced.

Generally one may divide the geometric imperfections into two categories; global imperfections and cross-sectional imperfections. Typically L/1000 (the exact value is L/960 based on Galambos (1998), but it is usually referred to as L/1000) is used as the magnitude and a global buckling mode shape is used as the distribution shape to approximate global imperfections.

[1] Post-Doctoral Fellow, Johns Hopkins University, <vahidzm@jhu.edu>
[2] Professor, Johns Hopkins University, <schafer@jhu.edu>

The common approach considering cross-sectional imperfections is to use a portion of the thickness of the members as the magnitude and the local and distortional buckling mode shapes as the distributionof these imperfections [Schafer and Pekoz 1998, Chou et al. 2000, Gardner and Nethercot 2004, Camotim et al. 2005, Ashraf et al. 2007, Dinis et al. 2007, Moen et al. 2010, Pham and Hancock 2010]. There are several research studies including measurements of imperfections [Ingvarsson 1977, Thomasson 1978, Dat and Pekoz 1980, Mulligan 1983, Lau 1988, Kwon and Hancock 1992, Bernard 1993, Schafer 1997, Young 1997, Shifferaw et al. 2010, Zeinoddini and Schafer 2011, Peterman and Schafer 2012] that are used in this study. The summary of the available imperfection measurements categorized into cross-sectional (local and distortional) and global (Bow or weak axis flexure, Camber or strong axis flexure and twist) are presented in Table 1.

Table 1: Statistical summary of available data on imperfections

	Local L (δ_0/t)	Distortional D (δ_0/t)	Bow G_1 (L/δ_0)	Camber G_2 (L/δ_0)	Twist G_3 (deg/m)
mean	0.47	1.03	2242	3477	0.36
st.dev.	0.62	0.97	3054	5643	0.23
25 %ile[(1)]	0.17	0.43	4755	6295	0.20
50 %ile	0.31	0.75	2909	4010	0.30
75 %ile	0.54	1.14	1659	2887	0.49
95 %ile	1.02	3.06	845	1472	0.85
99 %ile	3.87	4.46	753	1215	0.95

[(1)] %ile values are the probabilities that imperfection will be less than the table value

Different mode shape imperfections need to be combined in a proper way. The common approach is using the following equation:

$$f_0 = \sum_i \alpha_i C_i \phi_i \quad i\text{: mode shape} \tag{1}$$

In which f_0 is the imperfection field, α_i is the magnitude for each mode (can be chosen from Table 1, or traditionally chosen as 1/1000 of length or 10% of thickness), C_i is a coefficient to control the sign or portion of the mode imperfection that is input, and ϕ_i is the mode shape which is commonly normalized by deformation at a degree of freedom in the corresponding buckling mode shape (Figure 1b). Two approaches are introduced here; circle-SRSS (square root of the sum of the squares) and square-max. In circle-SRSS approach, the square root of the sum of the squares of the coefficients of the modes is set equal to one (Eq. 2) [Dinis and Camotim 2008, 2009, 2010].

$$\sqrt{\sum_i C_i^2} = 1 \tag{2}$$

For example, when the interaction of local and distortional modes is investigated imperfections are added as a combination of the local mode imperfection and distortional mode imperfection:

$$f_0 = \alpha_L C_L \phi_L + \alpha_D C_D \phi_D \tag{3a}$$

in which:

$$\sqrt{{C_L}^2 + {C_D}^2} = 1 \tag{3b}$$

This is better understood by considering the unit circle as in Figure 1. The other approach (square-max) is to consider the max values for each mode with different signs. In comparison to the circle-SRSS approach, this approach may be visualized as a square in the C_L, C_D plane with dimension of two as shown in Figure 1. The corners of the square are the desired combination cases, while the points on the axes correspond to pure mode imperfections (only one of the modes shapes exist). The "max" or square approach insures that the magnitude of a given mode is never less than what is measured, while the SRSS or circle approach presumes an interaction of imperfection mode shapes; when the magnitude of one mode increases, the magnitude of the other mode shape decreases. For imperfections which are actually buckling modes, and thus orthogonal, correlating the magnitudes with SRSS may be unconservative.

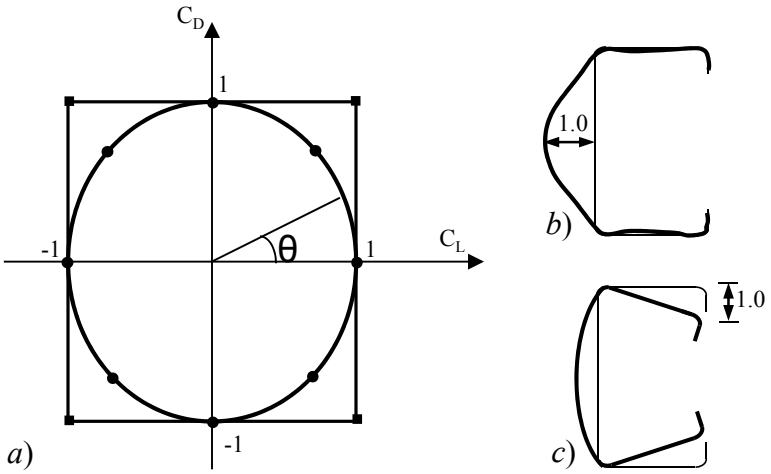

Figure 1: a) Square-max and circle-SRSS approaches to selecting magnitude when combining local (C_L) and distortional (C_D) imperfections. b) In square-max approach modes are normalized so that max(ϕ_i)=1. c) In SRSS approach modes are normalized so that the value at a specific degree of freedom is one. Note, these cross-sectional mode-shapes are distributed along the length over the critical length (Figure 3a and b)

2. Simulation Approaches

Three approaches for simulating imperfections in cold-formed steel sections are presented. The first one (Traditional Modal Approach) is a convenient approach yet based on real measurements. The second approach (2D Spectra Approach) is a relatively complicated method which uses the measurement results to simulate new samples employing a two-dimensional power spectral representation method. The third approach (1D Modal Spectra Approach) is a combination of the two which is not as complicated as the 2D Spectra Approach but is tied to the physical reality in a frequency sense.

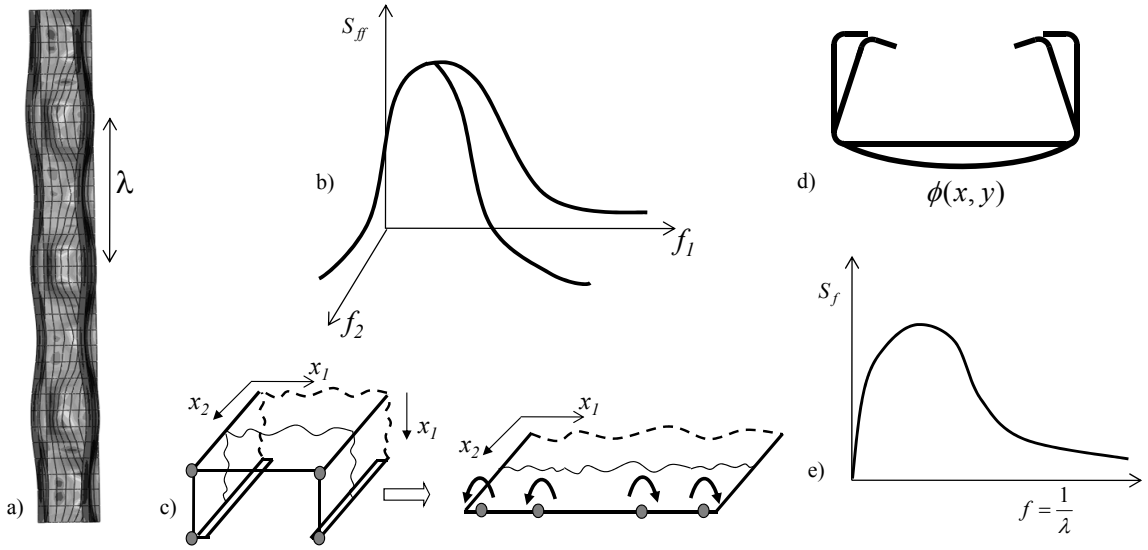

Figure 2: Three approaches for simulating imperfections, a) A mode shape and corresponding wave length in Traditional Modal Approach, b) A 2D spectrum, c) Transferring an imperfection field into a 2D field, d) A cross-sectional mode shape, e) A 1D spectrum -- α is the magnitude of imperfections, λ is the wave length for the imperfection mode, ϕ is the imperfection mode, S_f, S_{ff} are the magnitudes of 1D and 2D spectrums

2.1 Traditional Modal Approach

In the Traditional Modal Approach imperfections are modeled as a combination of buckling modes. The imperfection field, *f*, is:

$$f(x, y, z) = \sum_{i=1}^{5} \alpha_i . \phi_i(x, y, z) \tag{4}$$

where, α_i is the magnitude of each mode and ϕ_i is the mode shape (Figure 3). In this approach, the shape of the imperfection field comes from the mode shapes ($\phi_i(x, y, z)$). The mode shapes are obtained from an eigenvalue buckling analysis of the member, where the buckling mode shape corresponding to the lowest eigenvalue for each of the five modes is selected. (The mode shape is the outcome of a Finite Strip or Finite Element analysis and the shape is normalized so that the maximum deformation in each mode shape is one). The global mode shapes are pure flexural (weak axis and strong axis) and torsional modes and therefore relatively easy to obtain without buckling analysis. For each of these three modes the cross-section has a translation (G_1, G_2) or rotation (G_3) and the magnitude of this displacement (translation or rotation) changes along the length of the member as a half-sinusoidal curve. It should be noted that the proper combination of global modes is important, especially, G_2 and G_3 (flexural and torsional modes). The sign (positive or negative) of these modes can make a noticeable difference on their effect.

As in Eq. (4), to form the imperfection field, each normalized mode shape is multiplied by a magnitude (α_i). The magnitude of each mode is based on the available statistics of the measurements (Table 1). Depending on the level of confidence that is intended, a value from the table for each mode can be chosen. A common approach is to use 25%ile, 50%ile, and 75%ile values to investigate the imperfection sensitivity.

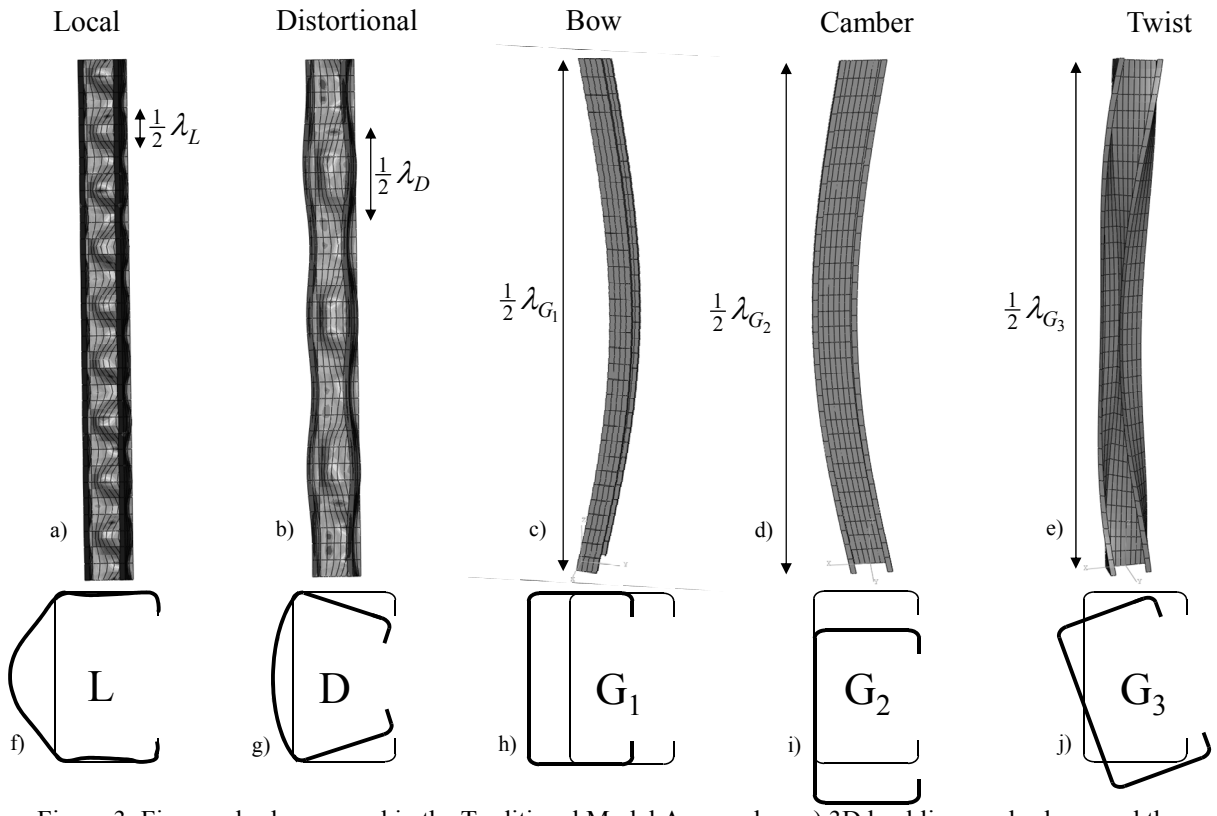

Figure 3: Five mode shapes used in the Traditional Modal Approach, a-e) 3D buckling mode shape and the corresponding wavelength, f-j) 2D cross-sectional mode shape, λ is buckling wavelength.

2.2 Random Field (2D) Spectra Approach

Imperfections change a great deal among different samples. Imperfections are to a great extent a random phenomenon and should be treated as such. Hence, imperfections may be understood as a random field superimposed on the "ideal" geometry of the cross-section. If the cross-section is "unfolded", one can consider it as a plate on which a two-dimensional (2D) imperfection field is imposed (Figure 2c). In a 2D Spectra Approach, two-dimensional spectral representation method is used to simulate samples of imperfections. For this, one needs a power spectrum based on expected imperfections such that new samples can be generated. This spectrum can be obtained from available data.

Consider the available imperfection data, $f_0(x,y,z)$, assigned to a plate as shown in Figure 2c, a 2D field, $f_0(x_1,x_2)$, is obtained after unfolding. The power spectrum of this field, $S_{f_0 f_0}(k_1,k_2)$ is calculated using Eq. (5) [Bendat and Piersol, 1971].

$$S_{f_0 f_0}(k_1,k_2) = \frac{1}{\Delta w_1}\frac{1}{\Delta w_2}\left|DFT(f_0(x_1,x_2))\right|^2 \tag{5}$$

In which k_1 and k_2 are the wave numbers in each direction, x_1 and x_2 are the location on the 2D plate, $\Delta W_i = 2\pi/L_i, i = 1,2$ where L_i is the length at each direction of the field, and $DFT(f_0)$ is the discrete Fourier transform of the field (f_0) [Bendat, Piersol, 1971]:

$$DFT(f_0(x_1,x_2)) = \frac{1}{N_1 N_2}\sum_{n_1=0}^{N_1}\left(e^{-2\pi i k_1 (n_1/N_1)} \sum_{n_2=0}^{N_2-1} e^{-2\pi i k_2 (n_2/N_1)} f_0(x_1,x_2) \right) \tag{6}$$

In which N_1 and N_2 are the number of discretizations in each direction. i is the imaginary unit.

After calculating the spectrum of each sample, the average spectrum of all samples (S_{ff}) is obtained. This is the spectrum based on which the simulation may be performed. Eq. (7) shows how the new samples are generated in a 2D spectral representation method [Shinozuka and Deodatis, 1996].

$$f(x_1,x_2) = \sqrt{2}\sum_{n_1=0}^{N_1-1}\sum_{n_2}^{N_2-1}\left[A_{n_1 n_2}\left\{ \cos(w_{1n_1}x_1 + w_{2n_2}x_2 + \Phi^{(1)}_{n_1 n_2}) + \cos(w_{1n_1}x_1 - w_{2n_2}x_2 + \Phi^{(2)}_{n_1 n_2}) \right\} \right] \tag{7}$$

in which

$$A_{n_1 n_2} = \sqrt{2 S_{ff}(n_1,n_2)\Delta w_1 \Delta w_2} \tag{7a}$$

$$w_{1n_1} = n_1 \Delta w_1,\ w_{2n_2} = n_2 \Delta w_2 \tag{7b}$$

$$\Delta w_1 = \frac{2\pi}{L_1},\ \Delta w_2 = \frac{2\pi}{L_2} \tag{7c}$$

$\Phi^{(1)}_{n_1 n_2}$ and $\Phi^{(1)}_{n_1 n_2}$ *; n_1 = 0, 1, ... N_1-1 ; n_2 = 0, 1, ... N_2-1* are sets of random phase angles distributed uniformly over the interval [0, 2π].

The generated two-dimensional fields, *$f(x_1, x_2)$*, need to be assigned to the original three dimensional shape of the section, *$f(x, y, z)$*. This is done by folding the plate back to the cross-section which is the reverse process of Figure 2c.

This approach can be closely tied to physical reality, but it is complicated for daily use and the assumptions needed for folding and unfolding process contradict with the original goal of being tied to physical reality. Therefore, an alternative approach is explored in the next section.

2.3 1D Modal Spectra Approach

In the proposed modal spectra approach, as Eq. (8) shows, the imperfection magnitude at each location in any cross-section along the length is a combination of the five cross-sectional buckling mode shapes (Figure 3f-j).

$$f(x,y,z) = \sum_{i=1}^{5} \alpha_i(z)\phi_i(x,y) \tag{8}$$

In which f is the imperfection field, $\alpha_i(z)$ is the magnitude of each mode at location z along the length of member, and $\phi_i(x,y)$ is the cross-sectional mode shape (Figure 3f-j). (Note, here ϕ_i is unlike the Traditional Modal Approach in which it is a function of x, y and z and instead the

imperfection field is decomposed into cross-sectional mode shape $\phi_i(x,y)$ and the magnitude along the length $\alpha_i(z)$). In this study the cross-sectional modes are derived from a finite strip buckling analysis of the cross-section using the software package CUFSM [Schafer and Ádány 2006].

For each mode shape, $\phi_i(x,y)$ is known from the buckling analysis of the cross-section. The magnitude of each mode along the length, $\alpha_i(z)$, is generated using the one-dimensional (1D) spectral representation method. This approach is a combination of the two previous approaches. In the longitudinal direction (z direction) the spectral representation method is used to generate the imperfection magnitudes. This means frequency content of the original data is considered in the longitudinal direction. But, in the transverse direction only the five mode shapes are considered. The benefits of this approach and how it ties the simulation to physical reality in a useful way will be discussed later in this section.

The spectral representation method requires a base power spectrum for the simulation. In this approach it is a 1D spectrum and it is derived from the available data. Since the data is decomposed into the five shown modal shapes, five base power spectrums (PSD's) are needed. To obtain these, first, the available measured data at each cross-section along the length is decomposed into the five mode magnitudes using least squared error. In other words at each cross-section along the length of member (in location z) the quantity $(\sum \alpha'_i \phi_i - f_0)^2$ is minimized to find $\alpha'_i(z)$ as the magnitude of ith mode in location z. In this term, f_0 is the measured imperfection values at the cross-section and α'_i and ϕ_i are the magnitude and the shape of ith mode respectively. For each measured imperfection sample, five processes corresponding to each of the five selected mode shapes are generated. The power spectrum of these 1D processes is found using equation (9) [Bendat, Piersol, 1971].

$$S_{f_0}(k) = \frac{1}{\Delta w}\left|DFT(\alpha'(z))\right|^2 \tag{9}$$

in which k is the wave number in longitudinal direction, $\Delta W = 2\pi/L$ where L is the length of the sample, and $DFT(\alpha')$ is the Discrete Fourier Transform of the 1D process (α') [Bendat, Piersol, 1971]:

$$DFT(\alpha'(z)) = \frac{1}{N}\sum_{n=0}^{N}\left(e^{-2\pi i k(n/N)}\alpha'(z)\right) \tag{10}$$

where N is the number of discretizations along the length.

The base PSD, S_f, for each mode is obtained by averaging the PSD's of the 1D processes corresponding to that mode for all available imperfection samples. Using one-dimensional spectral representation for each mode shape (Eq. 11), samples of 1D processes of magnitude of the mode along the length are generated. [Shinozuka, Deodatis, 1991].

$$\alpha(z) = \sqrt{2}\sum_{n=0}^{N-1}\left[A_n \cos(w_n z + \Phi_n)\right] \tag{11}$$

in which

$$A_n = \sqrt{2S_f(n)\Delta w} \tag{12}$$

$$w_n = n\Delta w \tag{13}$$

$$\Delta w = \frac{2\pi}{L} \tag{14}$$

and Φ_n*; n = 0, 1, ... N-1* is a set of random phase angles distributed uniformly over the interval [0, 2π] and z is the longitudinal location.

The above process is performed for each mode and, finally, the processes generated, $\alpha(z)$, for the five mode shapes are combined using Eq. (8) to generate a realization of an imperfection field. This procedure may be repeated to generate any number of samples. Note the PSD of each generated sample, in each mode, is equal to the PSD used to generate samples. However, the generated samples are different because of the randomness in phase angle (Φ_n).

2.4 Simulation of available data and comparison of approaches

In this section a set of imperfection measurements studied at Johns Hopkins University are used. 30 identical 8-foot-long studs (362S162-68 [SSMA nomenclature, SSMA product technical information, 2001]) were measured. These measurements include imperfections at seven points across the cross-section and every 0.1 in. (2.5 mm) along the length. Figure 4 shows the location of measurements around the cross-section and along the cross section. Table 2 summarizes the statistics of the Peterman and Schafer's measurements categorized into the five imperfection mode shapes. (The least squares method is used to fit the data to the five buckling mode shapes to find the magnitudes of each mode). The three imperfection modeling approaches are investigated on the channel section (362S162-68) used in Peterman and Schafer (2012) measurements.

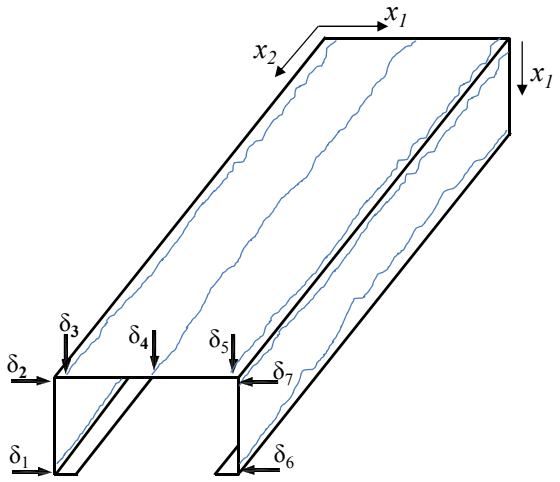

Figure 4: Imperfection measurement locations in and along cross-section in Peterman (2012)

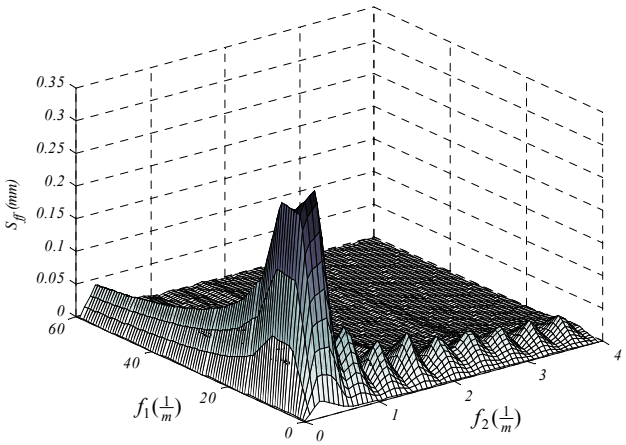

Figure 5: Average power spectrum of imperfections in Peterman 2012

Table 2: Statistical summary of measurements in Peterman and Schafer 2012

	Local L (δ_0/t)	Distortional D (δ_0/t)	Bow G_1 (L/δ_0)	Camber G_2 (L/δ_0)	Twist G_3 (deg/m)
Mean	0.48	0.89	1063	1337	0.36
st.dev.	0.24	0.43	2254	3861	0.20
25%ile	0.36	0.76	1421	1780	0.20
50%ile	0.47	0.84	1143	1381	0.36
75%ile	0.55	0.95	941	1197	0.46

2.4.1 2D Spectra Approach:

In this section the 2D Spectra Approach is used to simulate imperfection fields for the 362S162 channel section. First, the measured imperfections are used to find the original PSD to be used in the simulation. To obtain full imperfection field for each measured member, the imperfection values measured at each point are used as displacement loading on a perfect model in ABAQUS and linear elastic analysis is performed. The resulting imperfect member is unfolded to provide a 2D field of imperfections and the PSD of this field is obtained (Eq. 2). The same process is completed for all thirty samples measured in this program and the average PSD of all samples is obtained and used as the base PSD for simulations (Figure 5).

Finally, the 2D spectral representation method (Eq. 4) is employed to simulate new imperfection fields. Table 2 shows a statistical summary of the imperfections categorized into the five modes for 100 generated samples. The PSD of any of the generated samples is the same as the original PSD (Figure 5).

2.4.2 1D Modal Spectra Approach

In this section the 1D Modal Spectra Approach is used to simulate samples of imperfection fields for the 362S162-68 section. First, the magnitude of each of the five modes along the length is determined for all 30 samples. Power spectrum of each of the resulted 1D processes is calculated and the average PSD for each mode is found. These average PSDs are plotted in Figure 6. They are the base PSD's for generating new samples using the 1D spectral representation method.

Comparison of the statistical summaries of the generated samples using the 2D Spectra and 1D Modal Spectra Approaches to their corresponding measurement statistics (Figure 7) shows that the statistics for samples generated by 1D Modal Spectra Approach are more similar to the measurement statistics. As the figure implies the 1D Modal Spectra Approach captures the statistical values of the measured data more accurately in both cases. The 2D Spectra Approach does not capture the statistics of the global mode shapes accurately and this is a result of the error built in the folding and unfolding process in to the 2D Spectra Approach.

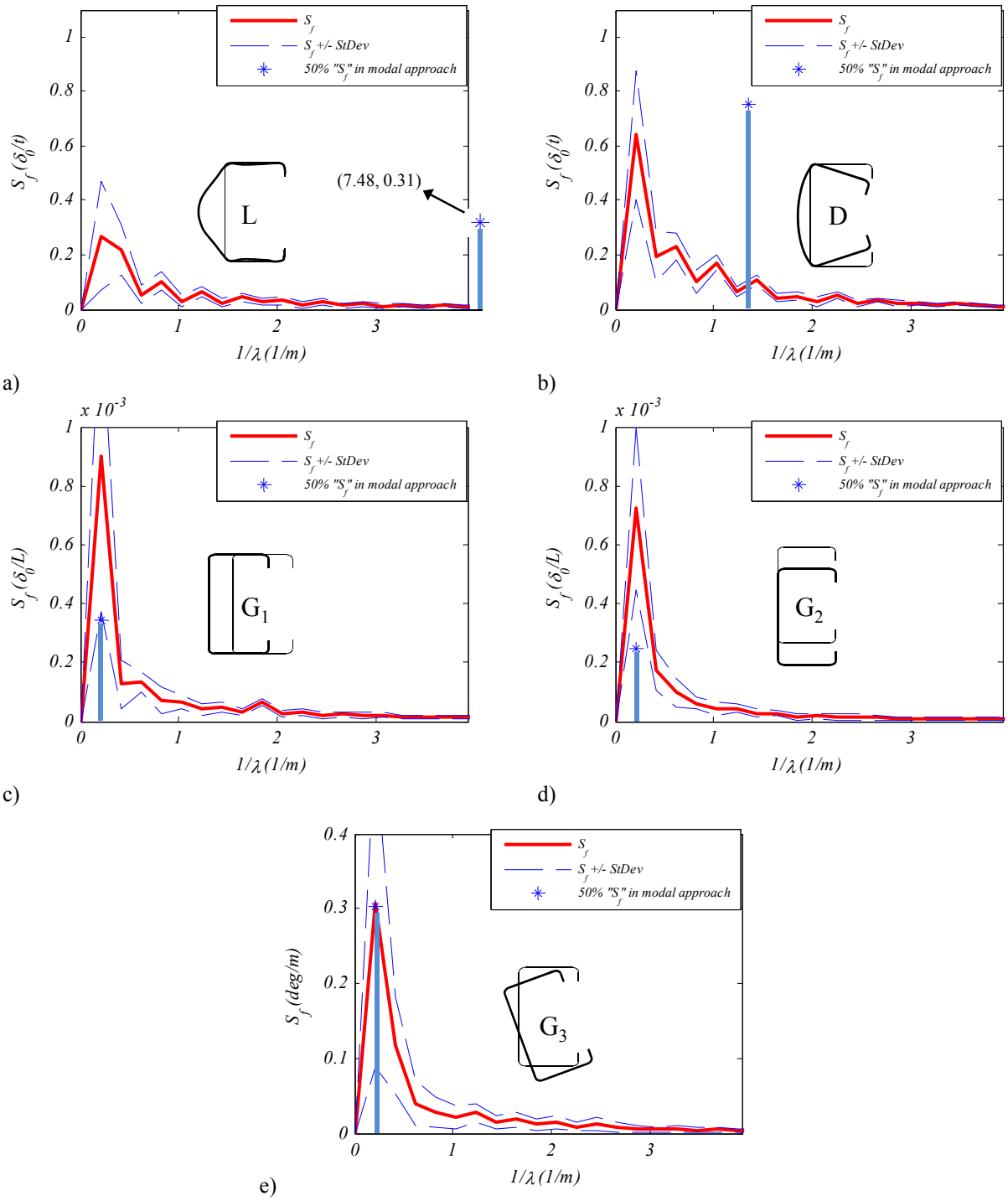

Figure 6: Average PSD (Base PSD) for modes 1-5 for 362S162 case, a) local mode, b) distortional mode, c) weak axis flexure, d) strong axis flexure, e) twist

To compare the 1D Modal Spectra Approach with the Traditional Modal Approach a study was performed to compare the frequency content of the real measurement data along the length (which is captured in the 1D Modal Spectra Approach) to the frequency content that the Traditional Modal Approach captures. Using the critical buckling length of each mode as the half

wavelength of the local and distortional mode shapes as in the Traditional Modal Approach does not agree well with the measurement data (the star (*) in Figure 6a and b). However, for the global imperfection modes since the frequency content is mostly around the frequency of the global buckling modes, the Traditional Modal Approach is a reasonable estimate (the star (*) in Figure 6c, d, and e). Thus, to tie the simulated imperfections to the physical reality of the measured imperfections, the 1D Modal Spectra Approach is a better tool compared to the Traditional Modal Approach. Note that recognizing the Traditional Modal Approach is typically an attempt to be conservative, as opposed to connecting intimately to physical reality.

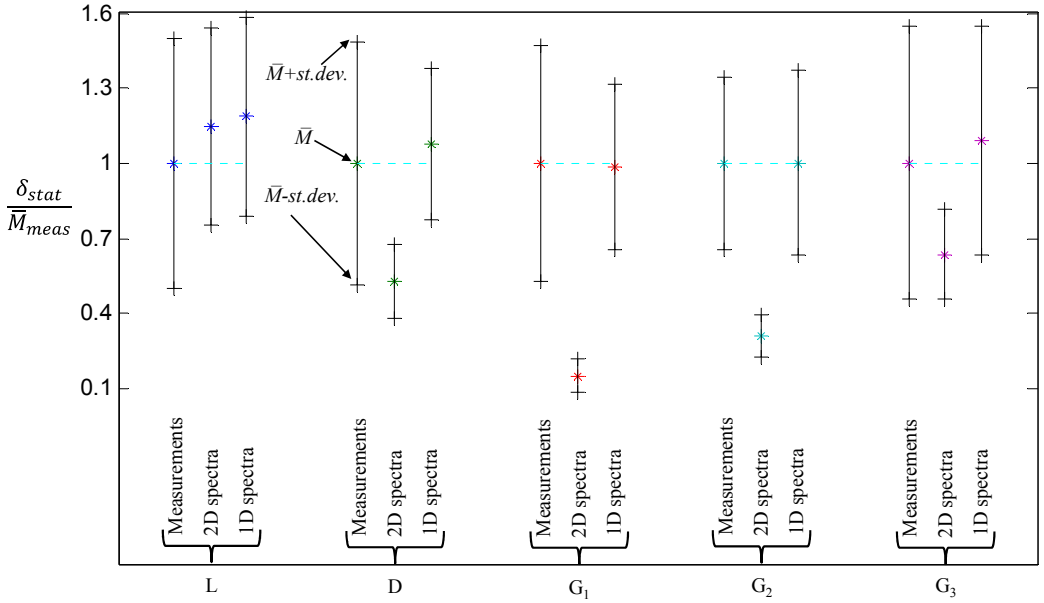

Figure 7: Comparison of the statistics of generated samples using 1D and 2D Spectra Approach to measurement statistics for 362S162 case. Note, all statistical values are normalized by the mean of measurements (Y-axis label).

3. Strength sensitivity to imperfection modeling approach

The different imperfection modeling approaches introduced and explained in the previous section are employed here to generate shell finite element models of the 362S162-68 member in ABAQUS. Collapse analysis i.e., geometric and material nonlinear analysis on the imperfect member (GMNIA) is performed.

3.1 The finite element model

The finite element package, ABAQUS (2007), is used for analysis. The ABAQUS shell element, S4R, is employed throughout. Fixed-fixed end boundary conditions are modeled; specifically, a reference node at the centroid of the cross-section at each end is defined and all the displacements of all other nodes at that end are tied to the reference node. All degrees of freedom of the reference node are restricted except longitudinal direction.

Compressive displacement loading is applied by moving the reference nodes towards one another. The modified Riks method [Crisfield, 1981] is chosen as the solution method. Material properties are based on a coupon test performed for the same section at Johns Hopkins University [Vieira 2011], Yield stress is considered as 388 MPa and ultimate stress is 652 MPa. An elastic modulus of 203000 MPa and Poisson's ratio of 0.3 is used.

Three elements for each lip width, 6 elements for each flange width, and 12 elements for the web depth, and 200 elements along the length of the member are used. The 362S162-68 has a 62.1 mm web, 41.3 mm flanges, and 12.7 mm lips, and 1.7 mm thickness. Element aspect ratios resulting from this discretization are 2.9, 1.8, and 1.6 for lip, flange and web elements.

The same cross-section (362S162-68) with the same length of 2.44 m (8 feet) is used in all cases. Four failure modes are explored. To change the failure mode, different bracing configurations are considered (Figure 8). The existence of braces, or spacing between the braces, differs in each model and causes different failure mechanisms.

There are three springs modeled at each "braced" point; two transitional springs in the direction of the two perpendicular cross-sectional axes and one rotational spring about the longitudinal axis. The stiffness used for springs is based on Vieira (2011) and corresponds to OSB sheathing. The values are: k_{x1}= 0.3738 N/mm, k_{x2}= 970 N/mm, k_{θ}= 0.0945 kN·m/rad.

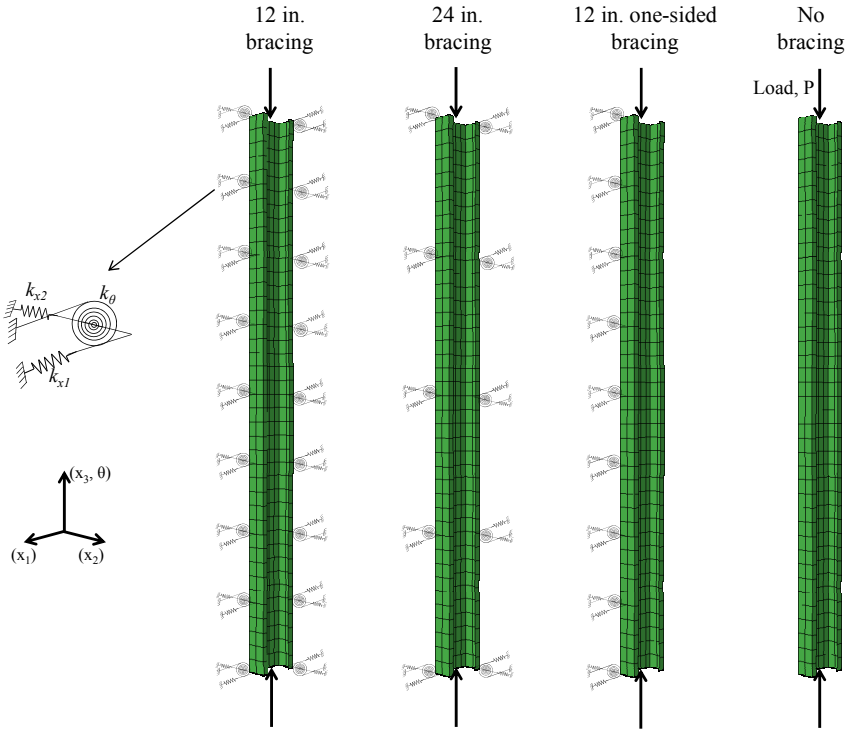

Figure 8: Bracing configuration for studied models (all models have fixed-fixed end boundary conditions)

As expected these four types of bracing cause different failure mechanisms in the models. For instance, if the failure mechanisms for one case of imperfections in the four types of models are compared (Figure 9), the difference in the behavior of each type is noticed. These plots correspond to models with different bracing configurations but the imperfection field is constant across the four models as the summation of 50%ile magnitude of all five imperfection mode shapes (the Traditional Modal Approach).

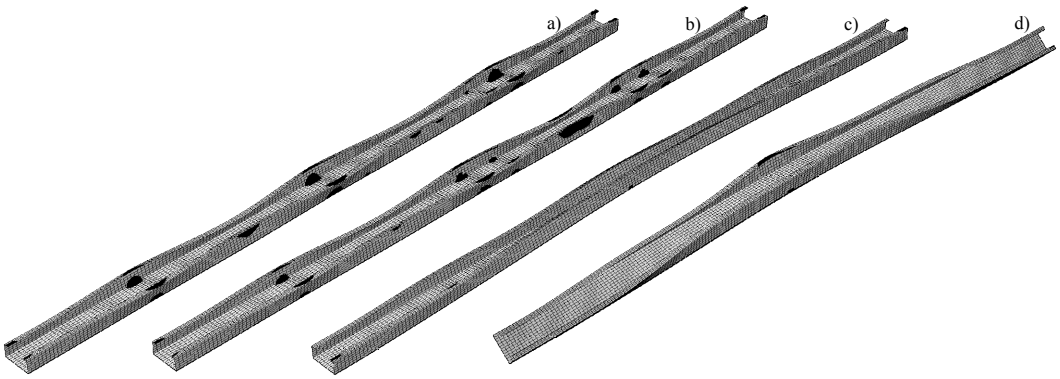

Figure 9: Sample of failure mode plastic strain contour plots for four types of models, a) 12 in. bracing, b) 24 in. bracing, c) 12 in. one-sided bracing , d) No bracing

In addition to the general results that are usually investigated in collapse modeling (i.e, peak load and load-displacement curve), a new parameter and a new type of plots are introduced and investigated in this study. Axial flexibility (k_a) is a parameter defined based on the end displacement at peak, Δ_p. Δ_p is the distance that the ends moved toward one another at the P_{max}. To compare Δ_p across samples, it is normalized by the expected axial shortening of the member under the peak load.

$$K_a = \frac{\Delta_p}{P_{\max} L / EA} \tag{15}$$

in which K_a is referred to as axial flexibility, L is the length of the member, E is the modulus of elasticity, and A is the area of the cross-section. This value, K_a, is representative of how much the imperfection and collapse soften the member axially.

To visually illustrate the location of the failure along the length, the portion of yielded elements at each longitudinal location is plotted over the length of members. For instance, if the plastic strain contour for a member at peak is as given in Figure 10a, the plot of the portion of yielded elements along the length would be as shown in Figure 10b. This plot allows for averaging over several samples which is important in this study.

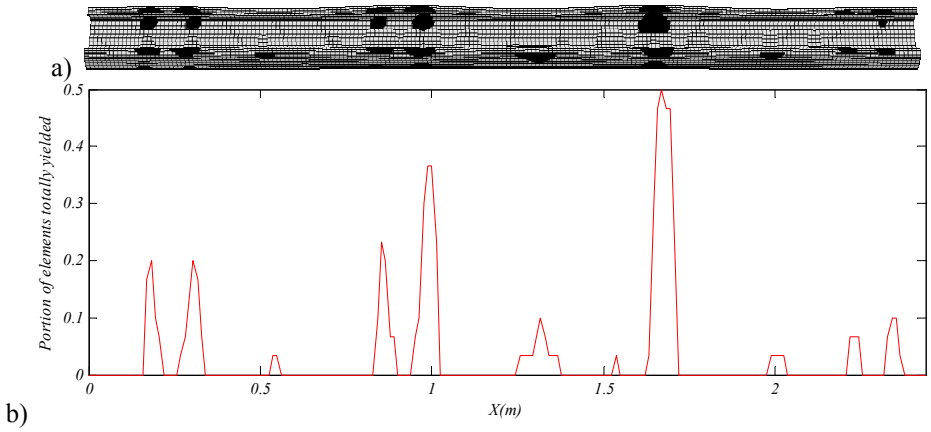

Figure 10: Failure mechanism for a sample model, a) plastic strain contour plot, b) portion of yielded elements in a given cross-section provided along the length of the model

3.2 Results of collapse modeling

In this section the results of applying the three approaches for simulating imperfections on different models are investigated. The results that are investigated include the peak load (P_{max}), axial flexibility (K_a), and portion of yielded elements along the length to investigate the collapse mechanisms. The results of different imperfection modeling approaches are compared against the models with as-measured imperfection. In these models, imperfections are input directly as they are measured in Peterman and Schafer (2012).

For Traditional Modal Approach, different magnitudes and signs for combining the local, distortional and global mode shapes are investigated. 50 percentile values (based on all the available measurement data, summarized in Table 1) are used. All 27 possible combinations for C_L C_D, and C_G in square-max approach (Figure 1) are considered. These possible combinations are shown via 3D illustration as solid circles in Figure 11. Note that the global mode shape includes Bow, Camber, and Twist and when C_G=1, all three (G_1, G_2, G_3) exist with positive sign, when it is zero neither of three exist, and when C_G=-1, all three exist with a negative sign. Positive and negative mode shapes are conventionally defined and cross sectional deformed shapes in Figure 3f-j show the positive mode shapes. To investigate the imperfection sensitivity two models with 25% and 75%ile values for mode imperfections in which all three modes have positive signs (C_L= C_D=C_G=1) are also analyzed.

A visual illustration of the peak load values for these 27 models is provided in Figure 12. Each solid circle represents the strength of the corresponding model in Figure 11. The third dimension (G) is represented by different markers introduced in the legend. The distance from each circle to the origin is proportional to the strength of the corresponding model (the distance to origin is equal to $\sqrt{C_L^2 + C_D^2} \cdot P_{\max}$). The dashed and dotted squares represent the strength of models with 25%ile and 75%ile imperfection values for all modes.

It is observed from Figure 12 that in models with 12 in. and 24 in. bracing, Global imperfections almost have no effect and as their coefficient changes from -1 to 0 and to 1 the strength of the models does not change. This story is very different in models with 12 in. one-sided bracing and no bracing where the global imperfections change the strength of models, especially in models with no bracing when no global imperfections exist (C_G=0) the strength of models increases significantly. Models with 12 in. bracing and models with 24 in. bracing have similar behavior which is a combination of local and distortional effects, although they were expected to fail in local mode and distortional mode respectively. The local and distortional mode imperfections have very similar effects in both cases. In models with 12 in. one-sided bracing, the opposite sign for global imperfections (C_G=1 vs. C_G=-1) effect the strength of models to some extent but in other cases the effect is very small. The effect of opposite signs for local and distortional mode imperfections is harder to judge in this figure, but overall one may conclude their effect (C_L=1 vs. C_L=-1 and C_D=1 vs. C_D=-1) is not very high which is justified through the fact that these members are relatively long (2.4 m). The imperfection sensitivity is noticeable in all four cases from the change of strength from 25%ile imperfections to 75%ile imperfections and is almost the same in all cases.

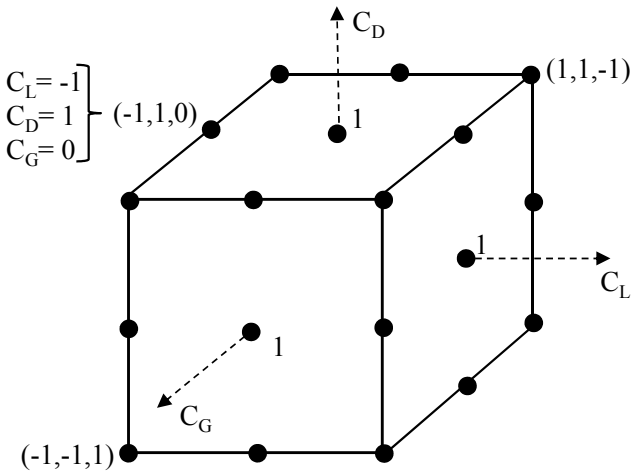

Figure 11: Illustration of different mode combinations for L/D/G in Traditional Modal Approach

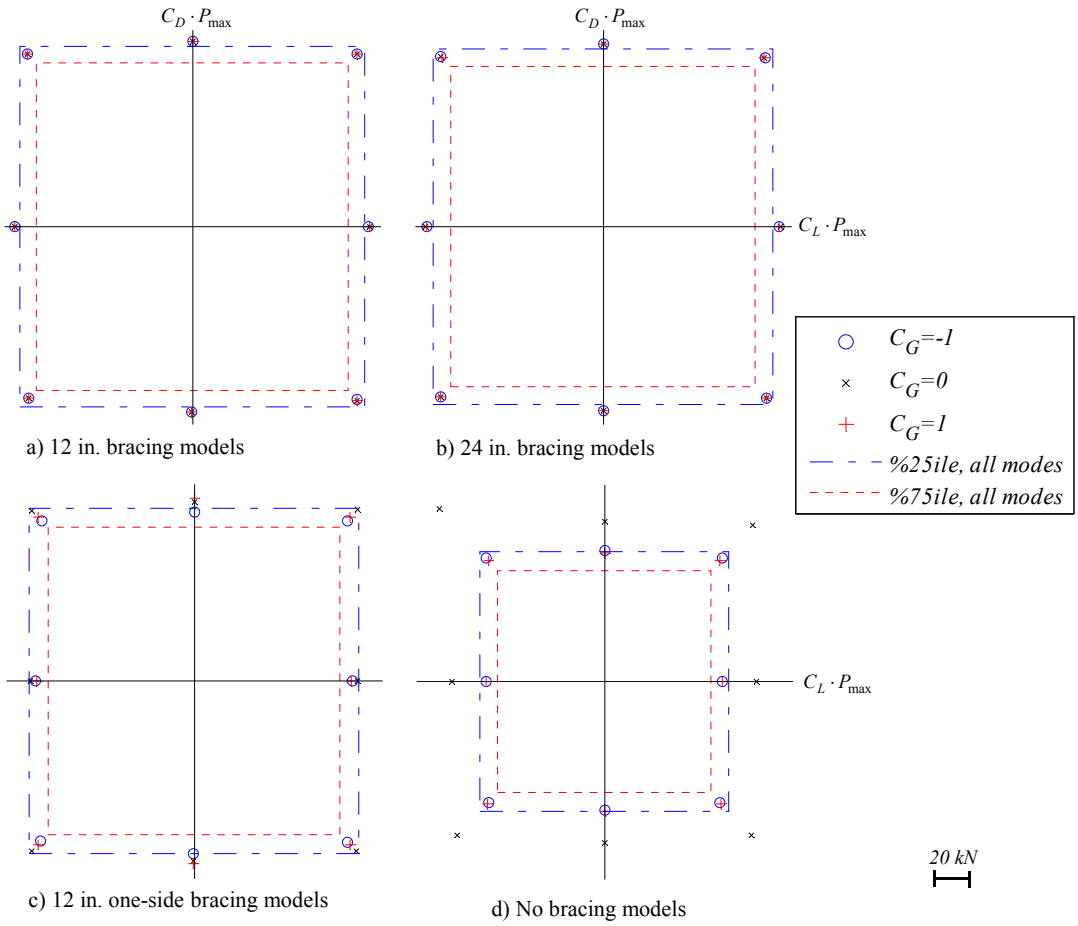

Figure 12: Illustration and comparison of strength when different combinations of L/D/G modes are used, a) C_G= -1, b) C_G= 0, c) C_G= 1.

It was observed that when the imperfection magnitude increases the axial flexibility increases (axial stiffness decreases). This is illustrated in Figure 13 which plots the P-Δ curve for models

with 25%, 50%, and 75% imperfection exceedance value of all modes. Although the peak load decreases, the end displacement at peak is increasing with larger imperfections meaning the members axially soften as they become more imperfect.

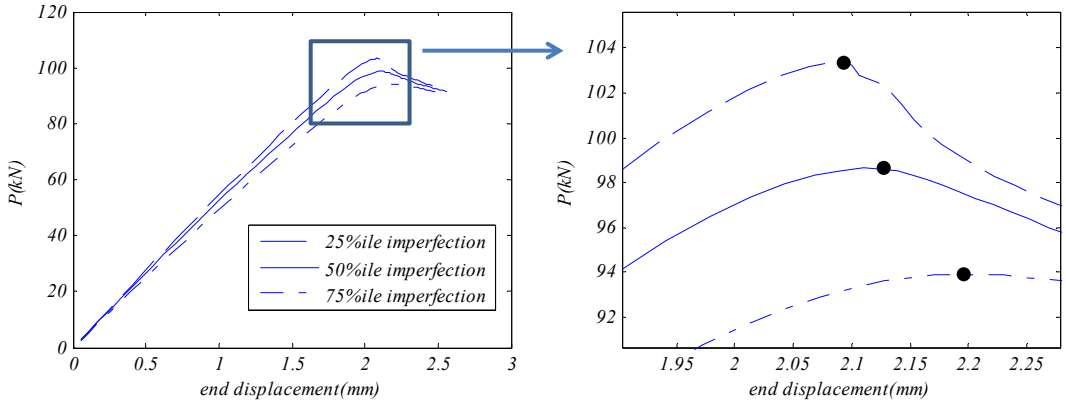

Figure 13: Peak load and end-displacement at peak for 25, 50 and 75%ile imperfection magnitudes in the Traditional Modal Approach for 12 in. bracing models

The results of collapse modeling using the three approaches (Traditional Modal, 2D Spectra, and 1D Modal Spectra) can be compared to the models with as-measured imperfections to evaluate the accuracy of each imperfection modeling approach in predicting the collapse behavior of cold-formed steel cross sections.

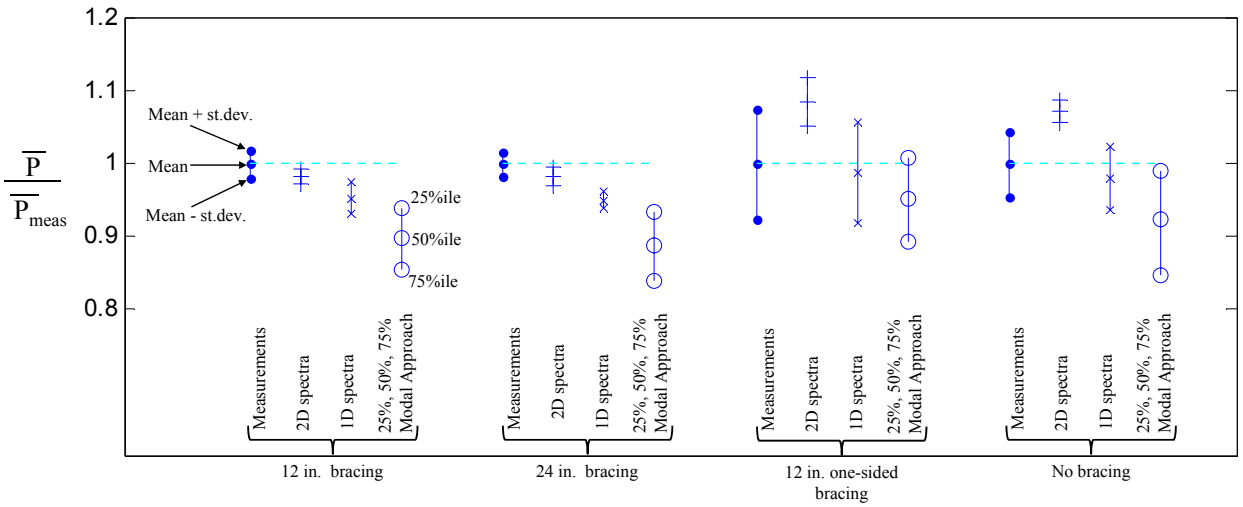

Figure 14: Comparison of P_{max} in different approaches

In Figure 14 the strength (P_{max}) predicted by the 2D Spectra Approach, 1D Modal Spectra Approach, and the Traditional Modal Approach (cases with 25%, 50%, 75% exceedance imperfection values) are compared. The strength values are normalized by the mean strength of the as-measured models for each model type. As shown, the 1D Modal Spectra Approach is the most accurate approach, predicting the strength with less than 4% error in a conservative manner. The 2D Spectra Approach predicts the strength of models with local and distortional failure modes (12 in. bracing and 24 in. bracing) well, but when the dominating failure mode is global

(12 in. one-sided bracing and no bracing), its performance is poor. The Traditional Modal Approach is conservative in predicting the strength.

In Figure 15 the prediction of axial flexibility, K_a, by the three approaches is also compared. Both the 1D and 2D Spectra Approaches capture K_a within a 5% error. Here, again, the 1D Modal Spectra Approach is always on the conservative side.

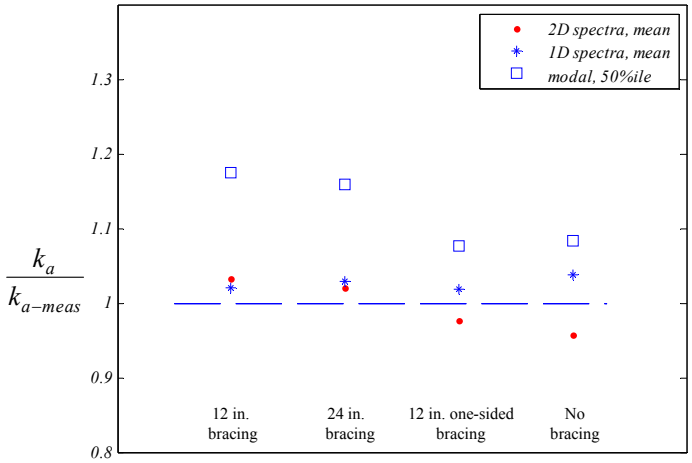

Figure 15: Comparison of axial flexibility (K_a) in different approaches

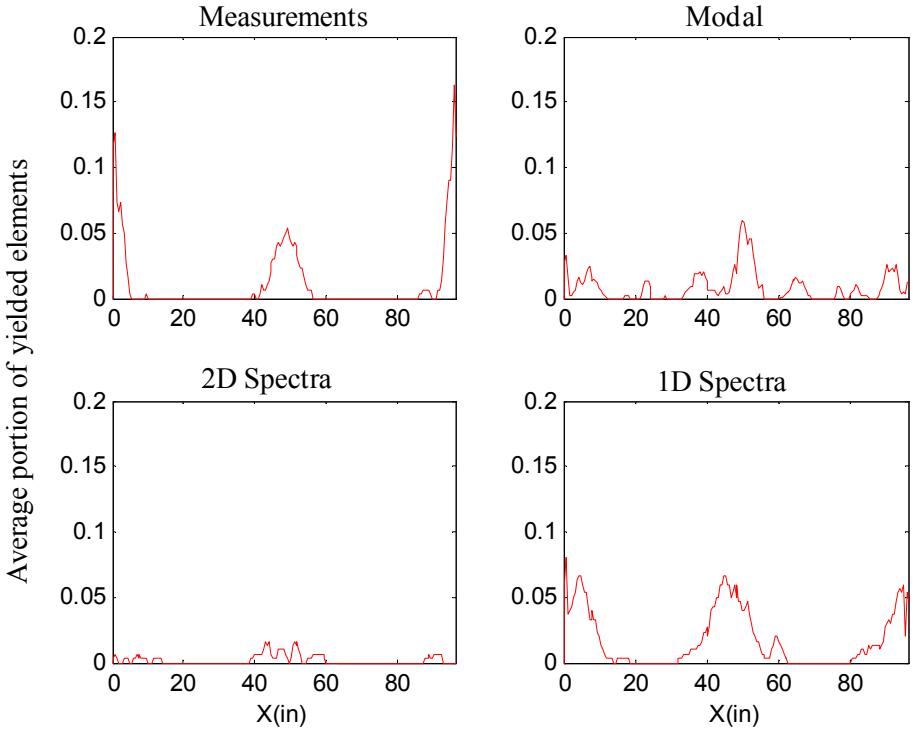

Figure 16: Comparison of failure mechanisms in different approaches for No-bracing models

Figure 16 compare the failure mechanism in three imperfection modeling approaches to the failure mechanism of the as-measured models for models with no bracing. It shows that the

failure mechanism is well-captured by the 1D Modal Spectra Approach, and does so more accurately than the 2D Spectra or Traditional Modal Approach.

4. Conclusions

A summary of the available data on cross-sectional imperfection and global imperfection measurements is presented. Three approaches for simulating imperfections (Traditional Modal Approach, 2D Spectra Approach, and 1D Modal Spectra Approach) are introduced. For a specific case of measured imperfection data these approaches are examined in generating the statistical summary of the measured data as well as in predicting the collapse behavior of the samples. A comparison of the generated samples using the 2D and 1D Modal Spectra Approaches shows that the imperfection distributions are better captured in the 1D Modal Spectra approach. The 2D Spectra Approach predicts the strength of models with local and distortional failure well, but when the dominating failure mode is global, it is less accurate. This is due to the fact that in this approach an error is introduced to the global mode imperfection content after folding and unfolding process. The Traditional Modal Approach is very conservative in predicting the strength. From collapse modeling, it is also concluded that the 1D Modal Spectra Approach is the most accurate approach for predicting the strength, axial flexibility, and failure mechanism of the member. The 1D Modal Spectra Approach is recommended for use in simulation.

5. References

ABAQUS (2007), ABAQUS/Standard User's Manual, Version 6.7, ABAQUS, Inc., Pawtucket, RI.

Ashraf, M., Gardner, L., Nethercot, D.A. (2007). "Finite element modeling of structural stainless steel cross-sections." *Thin-Walled Structures*, 44 (10) 1048-1062.

Bendat, J.S., piersol, A.G. (1971). "Random Data: analysis and measurement procedures." New York, Wiley, 1971.

Bernard, E.S. (1993), Flexural Behavior of Cold-Formed Profiled Steel Decking, Ph.D. Thesis, University of Sydney, Sydney, Australia.

Camotim, D., Silvestre, N., Dinis, P.B. (2005). "Numerical analysis of cold-formed steel members." *steel structures*, 5 (2005) 63-78.

Chou, S.M., Chai, G.B., Ling, L. (2000). "Finite element technique for design of stub columns." *Thin-Walled Structures*, 37 (2) 97-112.

Crisfield, M.A. (1981). "A fast incremental/iterative solution procedure that handles "snap-through"." *Computers & Structures*, 13 (1-3) 55-62.

Dat, D.T., Peköz, T.P. (1980). "The Strength of Cold-Formed Steel Columns." *Department of Structural Engineering Report*, Cornell University, No. 80-4, Ithaca, New York.

Dinis, P.B., Camotim, D. Silvestre, N. (2007). "FEM-based analysis of the local-plate/distortional mode interaction in cold-formed steel lipped channel columns." *Computers and Structures*, 85 (19-20) 1461-1474.

Dinis, P.B., Camotim, D. (2008). "Post-buckling behavior of cold-formed steel lipped channel columns affected by distortional/global mode interaction." Structural Stability Research Council, *Proceedings of the 2008 Annual Stability Conference*, 405-431.

Dinis, P.B., Camotim, D. (2009). "Local/Distortional/Global buckling mode interaction in cold-formed steel lipped channel columns." Structural Stability Research Council, *Proceedings of the 2009 Annual Stability Conference*, 295-323.

Dinis, P.B., Camotim, D. (2010). "Local/distortional mode interaction in cold-formed steel lipped channel beams." Thin-Walled Structures, 48 (10-11) 771-785.

Galambos, T.V. (1998). "Guide to Stability Design Criteria for Metal Structures." John Wiley & Sons, 5th Ed.

Gardner, L., Nethercot, D.A. (2004). "Numerical modeling of stainless steel structural components - A consistent approach." *Journal of Structural Engineering*, 130 (10) 1586-1601.

Ingvarsson, L. (1977). "Cold-Forming Residual Stresses and Box Columns Built Up By Two Cold-Formed Channel Sections Welded Together." Bulletin of The Department of Building Statics and Structural Engineering, 121, The Royal Institute of Technology, Stockholm, Sweden.

Kwon, Y.B., Hancock, G.J. (1992). "Strength Tests of Cold-formed Channel Sections Undergoing Local and Distortional Buckling." *ASCE Journal of Structural Engineering*, 118(7).

Lau, S.C.W. (1988). "Distortional Buckling of Thin-Walled Columns." Ph.D. Thesis, University of Sydney, Sydney, Australia.

Moen, C.D., Li, Z., Schafer, B.W. (2010). "Computational modeling of cold-formed steel." *Thin-Walled Structures*, 48 (10-11) 752-762.

Mulligan, G.P. (1983). "The Influence of Local Buckling on the Structural Behavior of Singly Symmetric Cold-Formed Steel Columns." Ph.D. Thesis, Cornell University, Ithaca, New York.

Peterman, K.D., Schafer, B.W., (2012). "Experiments of the stability of sheathed cold-formed steel studs under axial load and bending" American Iron and Steel Institute, Washington D.C., Ongoing research project, private communication, research report expected.

Pham C.H., Hancock, G.J. (2010). "Numerical simulation of high strength cold-formed purlins in combined bending and shear.", *Journal of Constructional Steel Research*, 66 (10) 1205-17.

Schafer, B.W. (1997). "Cold-formed Steel Behavior and Design: Analytical and Numerical Modeling of Element and Member with Longitudinal Stiffeners." Ph.D. Thesis, Cornel University, Ithaca, New York.

Schafer, B.W., Peköz, T. (1998). "Computational modeling of cold-formed steel: Characterizing geometric imperfections and residual stresses." *J. of Constructional Steel Research*, 47(3) 193-210.

Schafer, B.W. , Ádány, S. (2006). "Buckling analysis of cold-formed steel members using CUFSM: Conventional and constrained finite strip methods." *Eighteenth International Specialty Conference on Cold-Formed Steel Structures*, Orlando, FL.

Shifferaw, Y., Viera Jr., L.C.M., Schafer, B.W. (2010). "Compression testing of cold-formed steel columns with different sheathing configurations." Structural Stability Research Council, *Proceedings of Annual Stability Conference*, 593-612.

Shinozuka, M., Deodatis, G. (1991). "Simulation of stochastic processes by spectral representation." *Applied Mechanics Reviews*, 44 (4) 191-203.

Shinozuka, M., Deodatis, G. (1996). "Simulation of multi-dimensional Gaussian stochastic fields by spectral representation." *Applied Mechanics Reviews*, 49 (1) 29-53.

SSMA. Product technical information, ICBO ER-4943P, Steel stud manufacturers association, www.ssma.com, 2001.

Thomasson P. (1978). "Thin-Walled C-Shaped Panels in Axial Compression." Swedish Council for Building Research, D1.

Vieira, L. (2011). "Behavior and Design of Sheathed Cold-Formed Steel Stud Walls under Compression." Ph.D. Thesis, Johns Hopkins University, Baltimore, Maryland, USA.

Young B. (1997). "The behavior and Design of cold-formed channel columns." Ph.D. Thesis, University of Sydney, Sydney, Australia.

Zeinoddini, V.M., Schafer, B.W. (2011). "Global imperfections and dimensional variations in cold-formed steel members." International Journal of Structural Stability and Dynamics, 11 (5) 829-854.